Abatement of Emissions of a Residential Wood Stove

Laboureur, Marvin; Hannard, Maxence; Barakat, Tarek; Goel, Abhishek; Cornette, Jordi; Bram, Svend; Renard, Patricia; Duquesne, Thomas; Su, Bao Lian

Published in:
ACS Omega

DOI:
10.1021/acsomega.5c00854

Publication date:
2025

Document Version
Publisher's PDF, also known as Version of record

ACS OMEGA

Open Access

http://pubs.acs.org/journal/acsodf

Article

Abatement of Emissions of a Residential Wood Stove: Effect of the Catalyst on Gaseous and Condensable Pollutants Concentration and Their Toxicity

Marvin Laboureur,*◆ Maxence Hannard,◆ Tarek Barakat, Abhishek Goel, Jordi Cornette, Svend Bram, Patricia Renard, Thomas Duquesne, and Bao-Lian Su*

Cite This: *ACS Omega* 2025, 10, 25506−25517

Read Online

ACCESS | Metrics & More | Article Recommendations | Supporting Information

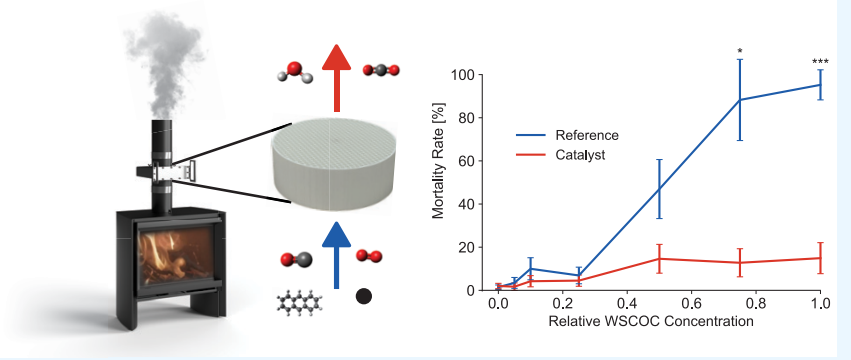

ABSTRACT: The use of biomass combustion for residential heating purposes is crucial for reaching the European Union's 2050 climate-neutrality goals. It, however, raises environmental and health concerns. This study explores the impact of a patented catalyst on wood stove emissions and, notably, its influence on cytotoxicity by comparing flue gas composition with and without the catalyst. Organic gaseous compounds (OGC) generated by wood combustion comprise two subgroups: water-soluble condensable organic compounds (WSCOC) and high-saturating vapor organic compounds (HSVOC). The second is mainly composed of methane, a molecule challenging to oxidize into CO_2 at these operating temperatures. While the catalyst moderately eliminates OGC (19%) in general, it excels in removing CO (87%) and WSCOC (80%), particularly polycyclic aromatic hydrocarbons (PAH) (91%). Bioassays on the A549 human cell line show that the catalytic WSCOC removal is correlated with a significant decrease in cytotoxicity (50%). Additionally, particle number size distribution measurements suggest that the catalyst facilitates the deposition of particles larger than 10 μm, leading to a 66% reduction in the particulate mass concentration. These results underscore the catalyst's role in mitigating harmful gaseous emissions and reducing the health risks associated with wood stove use, particularly by targeting toxic WSCOC.

1. INTRODUCTION

Used since the dawn of humanity, biomass combustion still has a bright future as a CO_2-neutral technology to achieve the objective of climate neutrality of the European Union (EU) for 2050.[1] Although biomass combustion does not contribute to an excess of CO_2 emission, improper combustion can release harmful compounds such as organic gaseous compounds (OGC), particulate matter (PM), and carbon monoxide (CO).[2−6] Depending on their composition, exposure time, and concentration, these compounds can have several impacts on humans and the environment. According to Cohen et al., PM from ambient air would be responsible for 4.2 million premature deaths because of their adverse effects on the human cardiovascular and respiratory systems as well as a result of the formation of cancer.[7]

The toxicological mechanisms behind PM-induced health effects are primarily driven by oxidative stress and inflammation of lung tissue.[8] Oxidative stress results from an imbalance between reactive oxygen species (ROS) production and antioxidant defenses, leading to cellular damage. This damage can manifest as (i) DNA damage, (ii) protein oxidation, and (iii) lipid peroxidation.[9] Polycyclic aromatic hydrocarbons (PAHs) present in PM can undergo metabolization into epoxide diols, which can subsequently form DNA adducts with

Received: January 28, 2025
Revised: April 16, 2025
Accepted: April 24, 2025
Published: June 11, 2025

nucleobases, such as adenine and guanine. The accumulation of these adducts can cause mutations, potentially leading to cell transformation or tumorigenesis.[10−13]

According to Cottom et al., residential wood-burning appliances are one of the primary sources of PM emissions from biomass combustion.[14] But emissions from wood-burning appliances exhibit considerable variability. For example, the emissions of $PM_{2.5}$ (particulate matter with an aerodynamic diameter ≤ 2.5 μm) per mass of burned wood of an open fire and a traditional stove stand at 12.1 and 6.2 g/kg, respectively, whereas a new-generation wood stove certified under the Ecodesign directive emits less than 2.1 g/kg of $PM_{2.5}$.[14,15] Primary measures were taken to achieve this clear reduction: Brandelet et al. have summarized the impact of using insulation, deflectors, secondary air and air-proof on the emission of pollutants.[16] Secondary measures can be considered as supplementary to engineering improvements in the removal of pollutants. Two main postcombustion technologies have been studied in the literature to remove pollutants emitted by a wood stove: catalytic oxidation,[17−20] which targets both gaseous and particulate pollutants and electrostatic precipitation,[19,21−23] which specifically removes only the solid phase of PM.

Catalytic oxidation remains one of the most promising techniques for pollutants removal. In the case of a wood stove, the residual heat in the exhaust is used to activate the catalyst and perform the oxidation of pollutants. Multiple laboratory-scale studies on synthetic gases have previously demonstrated the efficiency of catalytic oxidation toward the total oxidation of OGC and CO.[24−27] However, only a handful of studies have been conducted on real-time functioning wood stoves, where the composition of gases is far more complex. These studies have shown an effect on PAH[18] and on secondary organic aerosol (SOA) precursors.[17] Although the impact of oxidation catalysts on the chemical composition of fumes has been previously studied, their impact on the remaining cytotoxicity of the generated fumes has not yet been investigated.

The present work has the objective to characterize the performance of a patented catalyst (WO2020007949A1) on an 8 kW wood stove. The performance has been evaluated by measuring changes in the gas concentration (OGC, CO), particle number size distribution (PNSD), and total suspended particle (TSP) mass concentration, as well as by analyzing water-soluble condensable organic compounds (WSCOC). In addition, the in vitro cytotoxicity of fumes generated in the presence and absence of a catalyst treatment system has been investigated. The results of this study would represent a first holistic approach toward investigating the integration of a catalyst inside a wood-burning stove and its implications of the cleansing of the exiting fumes.

2. EXPERIMENTAL SECTION

2.1. Oxidizing Honeycomb Catalyst. The material used in this study was a Pt-loaded mixed ceria−zirconia catalyst, washcoated at the surface of a mullite ceramic honeycomb carrier provided by Rauschert GmbH. The coating of the mullite was prepared at the University of Namur (Belgium) according to the procedure described in detail in the WO2020007949A1 patent.[28] The physical data of the catalyst carrier are provided in Table 1.

The crystalline structure of the washcoat was investigated by X-ray powder diffraction (XRD) using a PANalytical X'Pert with Cu Kα_1 irradiation (λ = 1.5406 Å) and a 2θ angle scan from 10 to 80°. Additional XRD experiments were conducted on the washcoat, where data were collected on a Bruker D8 Advance X-ray powder diffractometer (Cu Kα radiation, Bragg−Brentano geometry, Eiger2R 500 K detector, fixed slits mode) with a 2θ angle scan from 15 to 120°. The resulting powder XRD pattern was refined using TOPAS V7 as a mixture of two crystal phases: cubic CeO_2 and cubic $CeZrO_4$. The unit cell parameters and microstructure parameters were refined.

Table 1. Physical Characteristics of the Ceramic Carrier

parameter	carrier
carrier type	mullite
cell shape	quadratic
cell density	25 cells/inch^2 (3.87 cells/cm^2)
carrier shape	cylindrical
diameter	15 cm
depth	5 cm

Scanning electron microscopy (SEM) measurements were carried out on a JEOL 7500-F instrument at 15.0 kV SEI WD 7.0 mm in order to investigate the morphology of the catalyst-coated surface.

2.2. Combustion Facilities. Combustion experiments were performed on an 8 kW 6-H 7660 wood-burning stove manufactured by Stûv S.A. (Belgium). To evaluate the catalyst, a retrofit box was mounted on the vertical flue gas outlet of the wood stove to ensure a sufficiently high temperature for the catalytic conversion of pollutants (Figure 1). In contrast to previous research,[29] the retrofit box was designed without a bypass as the evaluation of the catalyst's effectiveness included the high pollutant emissions during the warming-up phase (i.e., preload phase).

The performance of the catalytic wood stove was tested on a testing platform designed based on a EN16510 standard. The setup consists of a measurement section with a diameter of 150 mm installed above the stove where a draft (P_d) was continuously maintained at 12 Pa for all of the experiments (see Figure 1). Temperatures were measured with type K thermocouples (Tempco, 2 × 0.5 mm Glass Fiber 100 m spool). Temperatures downstream (T_d) and upstream of the catalyst (T_u) were measured inside the retrofit box in the center of the flue gas at respectively 2 cm below the catalyst (upstream) and 2 cm above the catalyst (downstream). Flue temperature at the sampling point (T_s) was measured in the center of the measurement section at the required distance based on the EN16510 standard. The monitoring of the pressure loss due to the catalyst (P_l) was measured with differential pressure transmitters (Furness, 0−5 Pa/0−50 Pa) where the pressure taps have been installed on the retrofit box at 2 cm below and above the catalyst.

2.3. Combustion Procedure. The appliance was operated according to the procedure detailed by the wood stove manufacturer and used to pass the certification EN16510. The combustion experiment is divided into two parts, preload and load, each divided into multiple combustion cycles as the wood stove is operated in batches. Three preload cycles are used to warm the wood stove to its nominal temperature (±350 °C). Then, five nominal load cycles are conducted for technical replicates. The detailed procedure containing the type and weight of wood used for preloads and loads is as follows. The first preload (P1) is made of 1000 g of spruce ("*Picea abies*") kindling arranged in "a Jenga tower" shape, the second preload

https://doi.org/10.1021/acsomega.5c00854
ACS Omega 2025, 10, 25506−25517

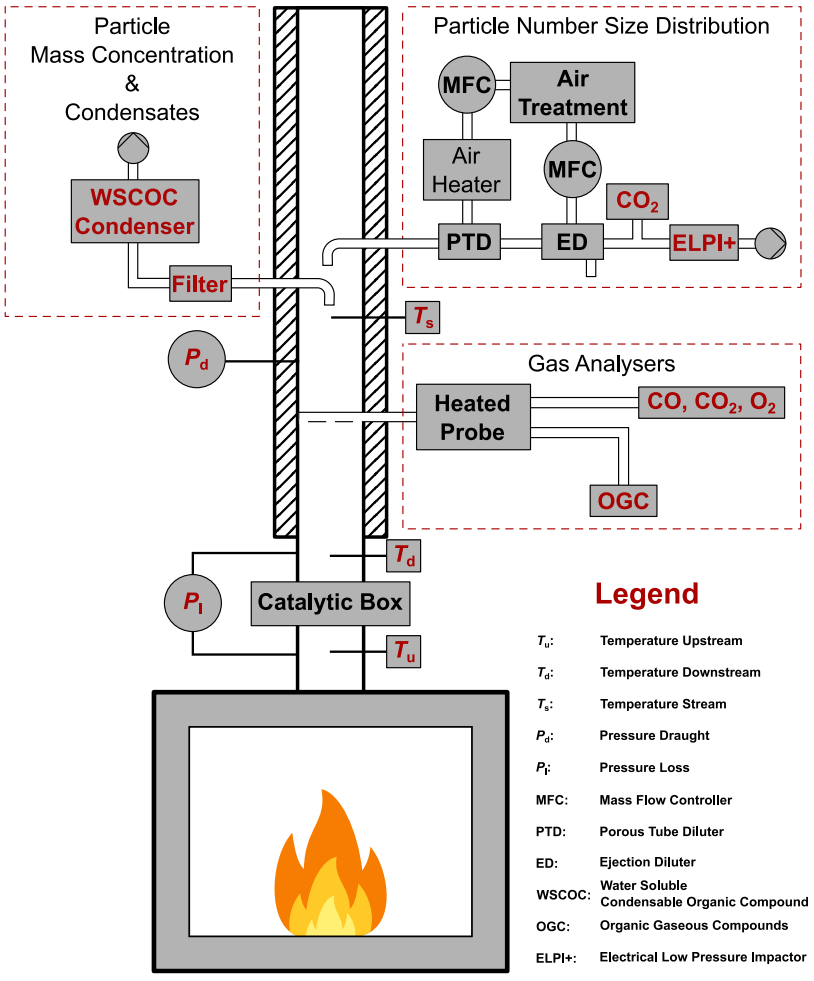

Figure 1. Schematic of the wood stove with measurement equipment.

(P2) is made of 2000 g of beech (*"Fagus sylvatica"*) middle-sized kindling with a length of 33 cm and a diameter of 3 cm. Finally, the third preload (P3) is made of 2000 g of sliced beech logs with a thickness of 3 cm. The five nominal loads (L1−5) comprise each of two logs of beech, 33 cm in length, a front log weighing 1100 g, and a rear log weighing 900 g. The humidity and the weight of the wood are measured before combustion using a Wöhler HBF 420 moisture meter and a Brecknell 405 scale, respectively. To ensure the comparison and the effect of the catalyst on the exhaust, measurements were conducted in the presence (named Catalyst) and absence of a catalyst (named Reference) in the catalytic box.

2.4. Characterization of Wood Stove Emissions. Gas-phase composition was continuously monitored using a Siemens Ultramat 6 (NDIR for CO_2 and CO), a Siemens Oxymat 6 (paramagnetic for O_2), and a FIDAMAT 6 (FID for OGC in methane equivalent) gas analyzers.

Particle size number distribution (PNSD) was also continuously monitored in the exhaust stream by using a Dekati electrical low-pressure impactor (ELPI+). Prior to ELPI + measurement, the gas sample was diluted in a two-stage dilution system, in accordance with the approach employed by Cornette et al.[30] The dilution system consists of a porous tube diluter (PTD) supplied at 17 L/min of clean air heated at 160 °C and an ejection diluter (ED) supplied at 45 L/min of clean air at room temperature. In order to determine the dilution ratio, the concentration in CO_2 was measured after the dilution system using a Vaisala GMP-343 CO_2 probe. The PNSD of particles with an aerodynamic diameter ranging from 6 nm to 10 μm was continuously monitored in the exhaust stream. Furthermore, a particle density of 2.0 g/cm^3[31] was assumed for ELPI+ data inversion, and impactor stages were equipped with oiled porous sintered collection plates due to their enhanced measurement stability compared to conventional aluminum collection substrates.[32]

WSCOC and particle mass were sampled using a slightly modified version of the Wöhler SM-96CO. Particles were sampled on a borosilicate cartridge (extraction sleeves, borosilicates Macherey−Nagel MN 649, diameter: 15 mm, thickness: 17 mm, height: 50 mm) placed in the heated sampling cane. The procedure was conducted before and after each sampling according to the instructions of the EN16510 standard. The sampling flow rate was preset on the Wöhler equipment at 9 L/min for 30 min, giving a flue gas volume (FGV) of around 270 L. Sampling was conducted during the nominal load cycles, starting 3 min after each reloading of the wood stove. The filter cartridge was dried at 120 °C for 1 h, then placed in a desiccant for 4 h, and finally weighed to determine the mass of the clean filter (Filter Weight empty—FW_e). Once sampling was complete, the filter was placed in a drying oven at 120 °C for 1 and 4 h in a desiccant before weighing the final mass of the filter (Filter Weight sample—FW_s). The final concentration of particles is corrected to 13 vol

https://doi.org/10.1021/acsomega.5c00854
ACS Omega 2025, 10, 25506−25517

% O_2 ($PM_{13\%O_2}$) by using the average concentration of O_2 during the cycle (O_{2avg}), and calculated based on eq 1

$$PM_{13\%O_2} = \frac{FW_s - FW_e}{FGV}\frac{21 - 13}{21 - O_{2_{avg}}} \quad (1)$$

The sampling of WSCOC was conducted by inserting an in-house-developed condensing system between the sampling cane and the pump. This system, adapted from Zotter et al. and their "sampling method 1", consists of two impingers, each containing 80 mL of distilled water that had been prefiltered using sterile syringe filters (ROTILABO MCE syringe filters, 0.22 μm) and one-third empty impinger placed right before the pump in case of spitting.[33] To decrease the vapor pressure of the compounds, all of the impingers were submerged in an ice bath. To ensure a concentration high enough to observe any short-term effect in the in vitro cytotoxic study, the condensate was sampled into the same water during the 5 nominal loads. At the end of the sampling, the condensates were collected and stored in a fridge at 5 °C away from any light source.

Chemical characterizations of WSCOC were outsourced to the BEAGx ("*Bureau Environnement et Analyses*"), a certified laboratory of chemical and microbiological analyses of environmental samples from the University of Liège (Belgium). Total organic carbon (TOC) and PAH concentrations have been measured by this laboratory in the condensates. The analysis focused on the 16 PAH list provided by the US Environmental Protection Agency (EPA), which is available in Table S2. These PAHs were chosen due to their frequent occurrence in environmental samples, their known toxicological profiles, and their importance as indicators of environmental contamination. Based on the FGV that went through the water and the final quantity of water (V_{water}), the concentration equivalent in STP condition (273.15 K and 1 bar) of WSCOC in the gas phase was estimated by eq 2. The concentration equivalent of PAH in the gas phase was also estimated by eq 2 using the PAH concentration in condensates instead of TOC

$$WSCOC_{STP\ 13\%\ O_2} = \frac{TOC \cdot V_{water}}{FGV}\frac{21 - 13}{21 - O_{2_{avg}}} \quad (2)$$

2.5. Cell Response Analysis. The A549, a human alveolar epithelial cell line derived from human lung carcinoma was selected for this study as it has been extensively used in airborne toxicity studies.[34−36] Cells were obtained from American Type Culture Collection (CCL-185 - ATCC, Rockville, MD) and were maintained in MEM medium culture containing Earle's salts and 25 mM of HEPES ("Gibco Minimum Essential Medium", ThermoFischer Scientific "Gibco") added with 10% fetal bovine serum ("Gibco Fetal Bovine Serum", Fischer Scientific), 1% nonessential amino acids (MEM NEAA 100×, Gibco) and 1% sodium pyruvate (Sodium pyruvate 100 mM, Gibco). They were maintained in the incubator (CellXpert C170, Eppendorf) at 37 °C and 5% CO_2. Expanding cells were maintained under 80% confluency and passed by using trypsin-EDTA ("Gibco Trypsin-EDTA (0.25%), phenol red", ThermoFischer Scientific). Cell cultures are routinely monitored for contamination to ensure the reliability and reproducibility of the experimental results. Specifically, a mycoplasma test is performed every 3 months (MycoAlert Mycoplasma Detection Kit, Lonza).

To expose A549 cell cultures to WSCOC under physiological conditions, it is necessary to convert the solution containing the condensates into a culture medium. First, 0.953 g of MEM powder ("Gibco Minimum Essential Medium powder", ThermoFischer Scientific) is dissolved in 90 mL of the condensate solution. Then, 2.66 mL of a 7.5% $NaHCO_3$ solution (99.7%, Sigma-Aldrich) is added to maintain the physiological pH and adjusted between 6.8 and 7.2. 1 mL of nonessential amino acids (MEM NEAA 100×, Gibco) and 1 mL of pyruvate (sodium pyruvate 100 mM, Gibco) are added to the solution. Finally, this solution is supplemented with 1 mL of streptomycin−penicillin ("Gibco Penicillin−Streptomycin (10,000 U/mL)", Fischer Scientific) and 10 mL of fetal bovine serum ("Gibco Fetal Bovine Serum", Fischer Scientific). The medium is then immediately filtered using a sterile filter with a porosity of 0.22 μm (Rotilabo syringe filter, Roth) and divided into 13 mL fractions in different centrifuge tubes (Corning 15 mL Centrifuge Tubes—Merck). These fractions are first flash-frozen in liquid nitrogen and then stored in a freezer at −80 °C until ready for use.

Cells were seeded on coverslips (MARI0117530, VWR) placed in 24-well plates at 5×10^4 cells/well for the live/dead assay for 24 h and seeded in a 12-well plate at 1×10^5 cells/well for the MTT (3-[4,5-dimethylthiazol-2-yl]-2,5 diphenyl tetrazolium bromide) assay. Afterward, cells are exposed for another 24 h to the culture medium prepared with 0, 5, 10, 25, 50, 75, and 100% of the WSOCO culture medium prepared as described above.

Cell viability is evaluated using the "Live−Dead" test ("LIVE−DEAD Viability/Cytotoxicity Kit" for mammalian cells, Invitrogen) following the manufacturer's recommendations. Briefly, a staining solution is prepared by adding 5 μL of calcein acetoxymethyl (AM), staining for live cells, 20 μL of ethidium homodimer-1, staining for dead cells, and 5 drops of "NucBlue Fixed Cell ReadyProbes Reagent—Invitrogen" (staining for nuclei) to 10 mL of culture medium. The medium from each well is replaced by 500 μL of the solution containing the fluorophores. After 20 min of incubation at 37 °C, the coverslips are mounted on slides (VWR Microscope Slides Cut Color Frosted White) and images are captured using a fluorescence confocal microscope (Leica TCS SP5) at a 10× magnification. In each micrograph, cells were counted after staining for each dye, including the number of dead cells (N_{dead}), the number of live cells (N_{live}), and the number of nuclei ($N_{nucleus}$), which serves as a proxy for the total number of cells (both dead and alive) in the sample. Subsequently, the mortality rate was calculated using eq 3

$$\text{mortality rate}[\%] = \frac{N_{dead}}{N_{nucleus}} \times 100 \quad (3)$$

Metabolic activity is assessed using the MTT test. Cells are incubated for 2 h at 37 °C in the presence of a mix of 500 μL of culture medium and 500 μL of freshly prepared MTT (2.5 mg/mL, "thiazolyl blue tetrazolium bromide", 98%, Acros Organics). The supernatant is removed, and 500 μL of DMSO (dimethyl sulfoxide, ≥99.5%, Sigma) is added to dissolve the formazan crystals. The plate is agitated at 37 °C for 1 h before reading the absorbance using spectrophotometry ("xMark Microplate spectrophotometer", Bio-Rad) at a wavelength of 550 nm. The metabolic activity was calculated based on eq 4 with the following parameters: the absorbance of the formazan formed in the well ($abs_{condition}$); the absorbance of DMSO

https://doi.org/10.1021/acsomega.5c00854
ACS Omega 2025, 10, 25506−25517

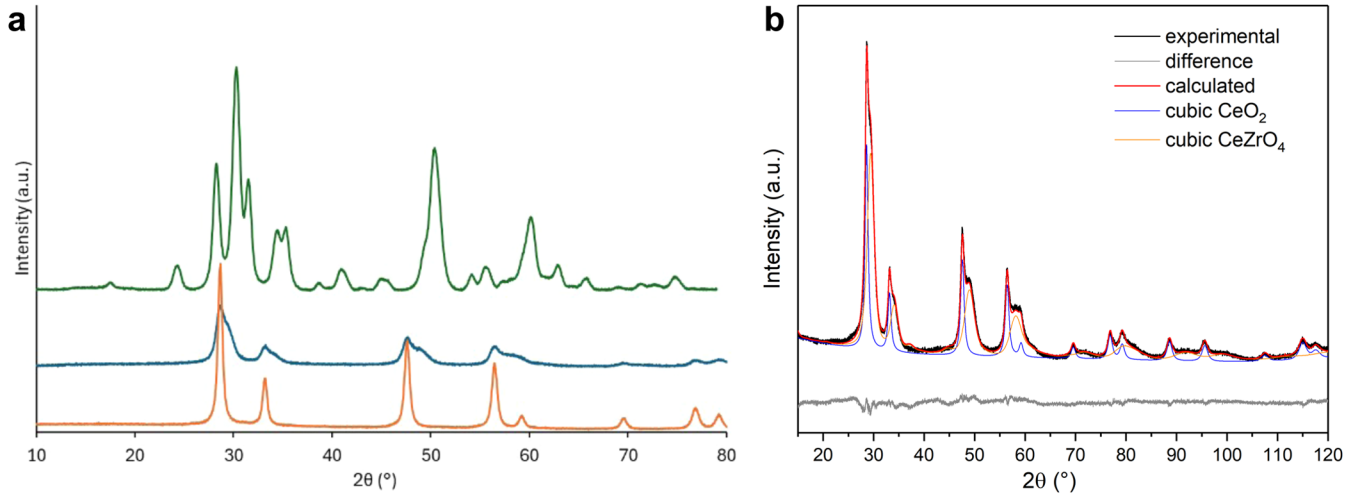

Figure 2. Powder XRD patterns of (a) washcoat material alongside ceria and zirconia for comparison purposes and (b) Rietveld refinement of the X-ray diffraction (XRD) pattern of the analyzed sample.

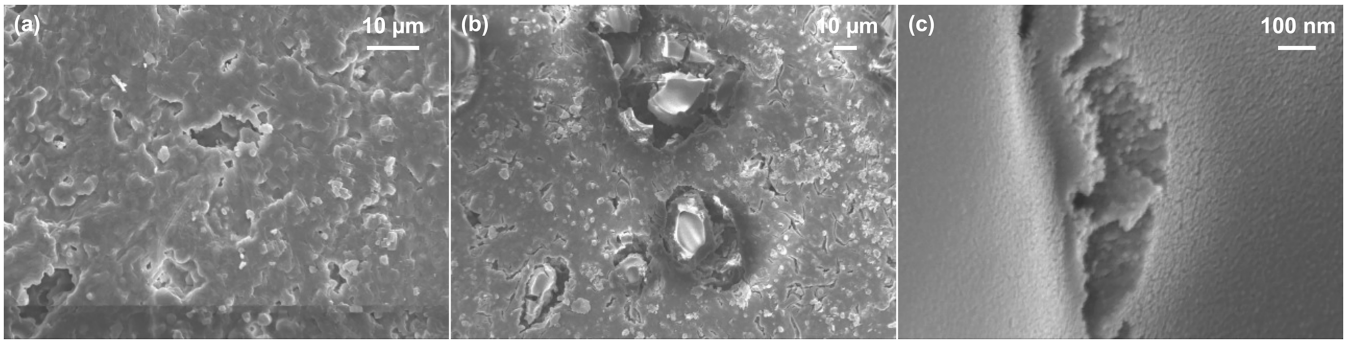

Figure 3. SEM Image of (a) bare mullite ceramic carrier, (b) washcoated mullite ceramic carrier, and (c) washcoated mullite ceramic carrier.

(abs_{blank}); and the absorbance of formazan formed in the well unexposed ($abs_{control}$)

$$\text{metabolic activity [\% control]} = \frac{abs_{condition} - abs_{blank}}{abs_{control} - abs_{blank}} \times 100 \quad (4)$$

2.6. Data Evaluation. The analyses of CO and OGC were done according to the EN16510 standard. The average emission concentration of each cycle was calculated and corrected to 13 vol % O_2 (STP) using eq 5, where X is CO, OGC, or TSP concentration, or PNSD determined by ELPI+

$$X_{avg\ 13\%\ O_2} = X_{avg} \frac{21 - 13}{21 - O_{2\ avg}} \quad (5)$$

The catalytic conversion for each measured pollutant was calculated using eq 6

$$\text{catalytic conversion [\%]} = \frac{E_{Reference} - E_{Catalyst}}{E_{Reference}} \times 100 \quad (6)$$

where $E_{Reference}$ is the average concentration emitted by the fireplace without the catalyst (Reference) and $E_{Catalyst}$ is the average emission when the fireplace is equipped with the catalyst (Catalyst).

All data and statistical analyses were performed using the R statistical programming language (Version 4.3.3). Welch's t test was used for pairwise comparisons of CO, OGC, and TSP due to the presence of unequal variances between groups. For particle distribution, a two-way ANOVA with interaction was conducted on log-transformed data. For mortality, a logistic regression was applied, with the survival rate as the response variable and treatment, dilution, and their interaction as explanatory variables. In the case of MTT, t tests were performed between the two treatments for each dilution, with the p-value correction applied using the Bonferroni method.

3. RESULTS

3.1. Catalyst Characterization. Prior to the coating of the ceramic carrier, the crystalline structure and morphology of the used washcoat was investigated. Powder XRD patterns of the washcoat material as well as those of CeO_2 and ZrO_2 (for the sake of reference) are illustrated in Figure 2a. The pattern of the washcoat exhibits well-defined broad peaks, which suggests that the synthesized CeO_2–ZrO_2 material is made of small-sized crystallites. Two crystalline phases can be identified in the pattern. A first glance at the pattern may suggest that the washcoat is composed of particles containing a mixture of CeO_2-rich and/or ZrO_2-rich crystalline phases. However, a more thorough investigation of the pattern revealed that the dominant crystalline phases are those of cubic CeO_2 and cubic $CeZrO_4$ (see Figure 2b). The peaks detected at 2θ angles of 28.1, 33.3, and 47.6° correspond to the cubic phase of ceria, whereas those detected at 28.8, 33.9, and 48.8° correspond to the cubic phase of cerium–zirconium oxide ($CeZrO_4$). The

https://doi.org/10.1021/acsomega.5c00854
ACS Omega 2025, 10, 25506−25517

Table 2. Averaged Results of Combustion Cycles, Including the 3 Preloads and 5 Loads, from Performance Analysis Tests in the Absence of the Catalyst (Reference) or in the Presence of the Catalyst (Catalyst)[a]

test	cycle		moisture content (%)	CO_2 (%)	O_2 (%)	CO (mg/Nm^3)	OGC (mgC/Nm^3)	TSP (mg/Nm^3)	WSCOC (mgC/Nm^3)	PAH (μg/Nm^3)	T_u (°C)	T_d (°C)	T_s (°C)	duration (min)
reference	preload 1	P1		5.3	15.4	2055	295[b]				170	146	120	16
	preload 2	P2	19.2	10.8	9.8	4514	746				350	310	258	33
	preload 3	P3	19.1	11.8	8.8	2411	302				393	352	303	36
	load 1	L1	18.9	9.0	11.8	865	103	38.4	39.5	122	366	331	294	52
	load 2	L2	18.6	7.7	13.1	1477	137	21.6			342	313	277	46
	load 3	L3	20.1	9.0	11.7	1028	155	19.4			358	325	283	48
	load 4	L4	19.4	8.3	12.5	1204	126	13.5			350	316	278	45
	load 5	L5	18.9	8.7	12.1	1364	274	25.2			350	315	278	46
	average loads	L-AVG	**19.2 ± 0.6**	**8.5 ± 0.6**	**12.2 ± 0.6**	**1187 ± 247**	**159 ± 67**	**23.6 ± 9.3**	**39.5**	**122**	**353 ± 9**	**320 ± 8**	**282 ± 7**	**47 ± 3**
catalyst	preload 1	P1		6.2	14.5	2723	433[b]				174	153	106	16
	preload 2	P2	19.8	11.3	9.5	1529	347				360	370	265	32
	preload 3	P3	19.9	11.7	8.9	320	194				391	373	295	32
	load 1	L1	19.4	7.9	13.0	166	111	5.6	7.8	10	352	328	273	43
	load 2	L2	20.5	8.9	11.9	216	255	6.5			357	334	272	51
	load 3	L3	19.6	8.9	11.9	128	103	7.1			362	333	272	45
	load 4	L4	20.3	9.4	11.4	113	68	6.4			371	338	274	49
	load 5	L5	17.8	9.5	11.2	137	109	13.6			383	350	283	42
	average loads	L-AVG	**19.5 ± 1.1**	**8.9 ± 0.7**	**11.9 ± 0.7**	**152 ± 41**	**129 ± 73**	**7.9 ± 3.2**	**7.8**	**10**	**365 ± 12**	**337 ± 8**	**275 ± 4**	**46 ± 4**
catalytic conversion	preload 2	P2				66%	53%							
	preload 3	P3				87%	36%							
	average loads	L-AVG				87%	19%	67%	80%	91%				

[a]Assessing wood moisture content as the mass of moisture per mass of wet wood and cycle duration; concentrations of CO_2 and O_2 in downstream exhaust, along with corrected levels at 13% O_2 of CO, organic gaseous compounds (OGC), total suspended particles (TSP), water-soluble condensable organic compounds (WSCOC), and polycyclic aromatic hydrocarbons (PAH) where the mass of each identified (16 EPA PAH) species was summed; temperatures recorded upstream (T_u) of the catalyst, downstream (T_d) of the catalyst, and in the stream (T_s) according to the EN16510 standard. OGC and WSCOC concentrations are expressed in mass of carbon per unit volume under standard temperature and pressure (STP) conditions (mgC/Nm^3). [b]Concentration in wet gas and not dry gas.

https://doi.org/10.1021/acsomega.5c00854
ACS Omega 2025, 10, 25506−25517

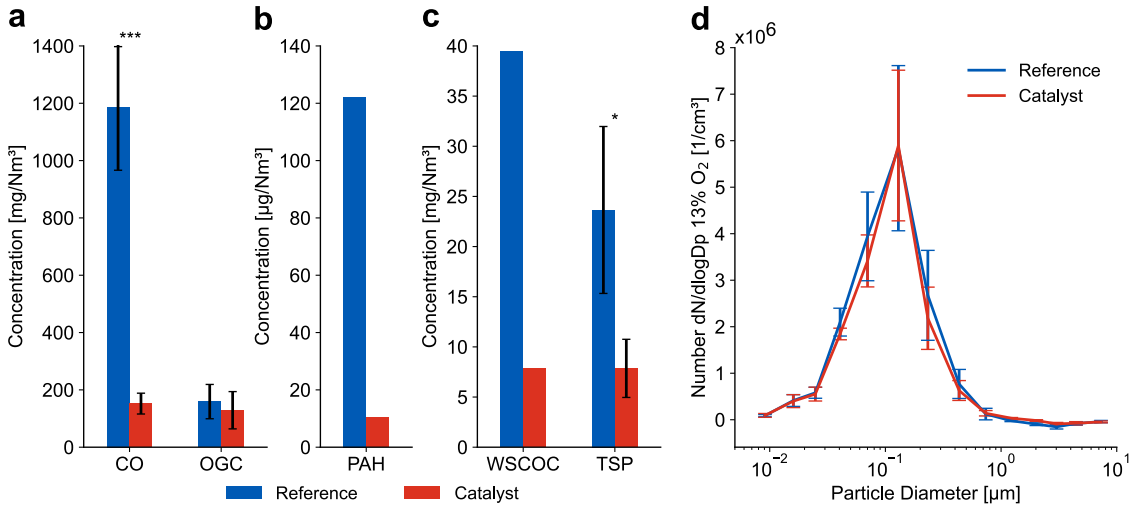

Figure 4. Average emission concentrations from the five loads (n = 5) corrected to an O_2 reference concentration of 13 vol% for (a) CO and organic gaseous compounds (OGC) based on carbon mass concentration; (b) polycyclic aromatic hydrocarbons (PAH) where the mass of each identified (16 EPA PAH) species was summed; (c) water-soluble condensable organic compounds (WSCOC) based on the total organic carbon mass concentration and total suspended particles (TSP); (d) particle number size distributions (PNSD) adjusted with the used dilution ratio. Each error bar symbolizes the standard deviation; PAH and WSCOC cumulative measurement over 5 cycles (n = 1). Statistical analyses were performed using Welch's t test used for pairwise comparisons of CO, OGC, and TSP due to the presence of unequal variances between groups and a two-way ANOVA with interaction was conducted on the transformed data for PNSD using R v4.3.0 software; $p < 0.05$ (*), $p < 0.01$ (**), $p < 0.001$ (***), and $p < 0.0001$ (****).

Rietveld refinement of the pattern using these two crystalline phases revealed an estimated content of 29 wt % for the cubic CeO_2 phase and 71 wt % for the cubic $CeZrO_4$ phase. The estimated crystal size is 8.7 nm for the cubic CeO_2 phase and 6.2 nm for the cubic $CeZrO_4$ phase. The lattice parameters of CeO_2 and $CeZrO_4$ phases are 5.4 and 10.5 Å, respectively.

SEM images of the bare and washcoated ceramic carrier are illustrated in Figure 3. Figure 3b reveals a surface made of a mixture of smooth and crack-filled zone. A magnification of the crack zones reveals that the surface is made of tightly packed spherical particles. Even though it is difficult to assess the exact size of these particles, Figure 3c shows that the size range of the catalyst particles is lower than 30 nm. The intimate contact between the particles forming the washcoat may also suggest an intimate contact between the coexisting crystalline phases.

From a catalytic point of view, the interest of forming a mixed cerium−zirconium oxide material lies in the incorporation of Zr species in the lattice, which promotes the mobility of oxygen, the thermal stability of the material, and the formation of oxygen vacancies.[37,38] In addition, loading of platinum species on CeO_2 and cerium−zirconium oxide materials has also been correlated to an increase in oxygen mobility. Marinho et al. describe that the intimate contact of Pt species with ceria and ceria−zirconia particles drastically increases "the oxygen exchange, demanding lower activation energy due to the higher metal−CeO_2 interaction".[39] This increase was most notable in the mixed ceria−zirconia material, helped by the extra presence of zirconia. The authors deduce that the intimate contact between Pt and the ceria or the ceria−zirconia supports facilitates the formation of reactive oxygen species. In this work, the small size of the particles constituting the washcoat, combined with the intimate contact between these particles and the presence of a dominant $CeZrO_4$ crystalline structure may constitute a reactive surface that, when loaded with platinum species, may offer the advantage of high oxygen mobility at the surface. This can be highly beneficial to the catalytic oxidation of carbonaceous pollutants at relatively low temperatures.

3.2. Gas Emission. The objective of this study was to evaluate the impact of a catalyst on wood stove emissions and its effect on the cytotoxicity of fumes throughout the entire test duration of a wood stove. Therefore, emissions were recorded during the warm-up phase (i.e., preload phase) and in the nominal load phase as specified in the EN16510 standard. The evolution of the emissions and temperatures throughout the combustion tests are presented in Figures S1 and S2. Averages of emission values collected from preloads and loads, and corrected to 13 vol % O_2, are shown in Table 2.

The temperature of the exhaust (and therefore of the catalyst) during the warm-up of the stove (P1) is not sufficiently high to show an effect of the catalyst on the concentrations of CO or OGC. After the first reloading operation (P2), the temperature increases rapidly to nearly 400 °C and consequently, a high conversion of pollutants is observed. During P2, the average catalytic conversions are 53% for the OGC and 66% for the CO. These conversions decrease to 36% for the OGC and increase to 87% for the CO during P3. These differences in catalytic conversion between CO and OGC have been previously reported in the literature[17,18] and are attributed to the presence of methane. Its high abundance and low catalytic conversion reduce the overall catalytic efficiency of the OGC group. The average emissions of CO and OGC during the five nominal loads have an average catalytic conversion of 87% (p = 0.0006) and 19% (p = 0.51), respectively (see Figure 4a).

Moreover, during the preload phases, the temperature downstream of the catalyst reached at one point 80 °C above the temperature upstream of the catalyst (see Figure S3b), meaning that a highly exothermic reaction is occurring and, in turn, is heating the exhaust. As the concentration of CO during this same phase can reach the upper limit of detection of our instrumentation (>10,000 ppmv), the catalytic oxidation of this high amount of CO toward CO_2 is the main reaction

https://doi.org/10.1021/acsomega.5c00854
ACS Omega 2025, 10, 25506−25517

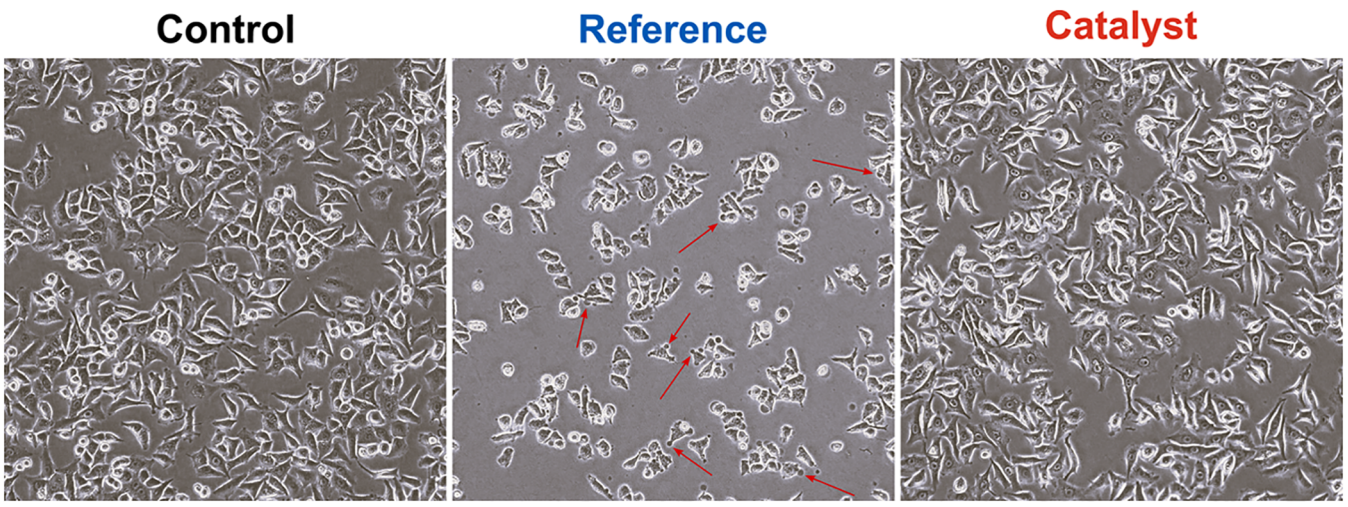

Figure 5. Phase-contrast micrographs of A549 cell lines at 10× magnification after being exposed or not (Control) to a relative concentration of 0.50 of water-soluble condensable organic compounds (WSCOC) in the absence of the catalyst (Reference) and in the presence of the catalyst (Catalyst) over a 24 h period. The red arrows indicate blebs present on the cells.

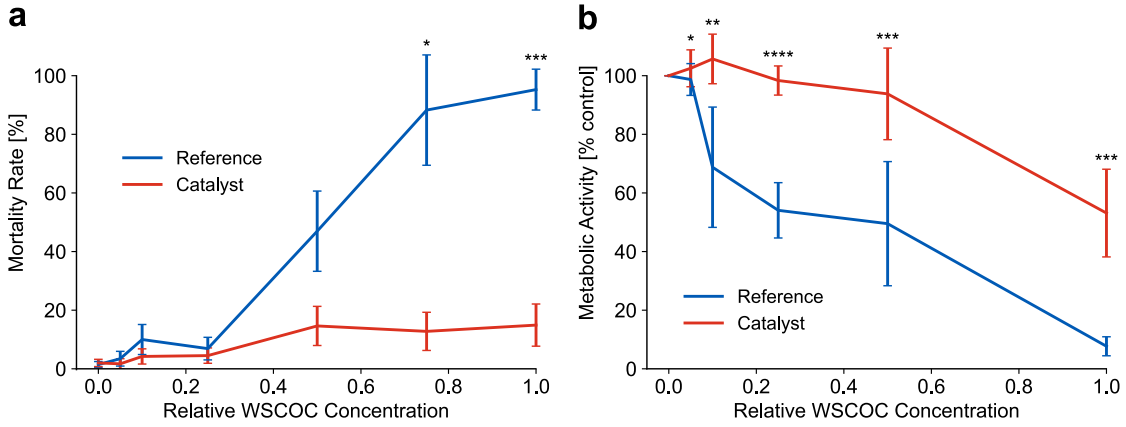

Figure 6. (a) Mortality of A549 cells induced by 24 h exposure to different relative concentrations of WSCOC (0.05 to 1) from Reference or Catalyst (n = 3 independent replicates). (b) Relative metabolic activity assessed by the MTT assay of A549 cells exposed for 24 h to different relative WSCOC concentrations (0.05−1) from the Reference or the Catalyst (n = 7 independent replicates), each error bar symbolizes the standard deviation, statistical analyses were performed using R v4.3.0 software using logistic regression, with survival rate as the response variable and treatment, dilution, and their interaction as explanatory variables for the live−dead assay. In the case of MTT, t tests were performed between the two treatments for each dilution, with p-value correction applied using the Bonferroni method. $p < 0.05$ (*), $p < 0.01$ (**), $p < 0.001$ (***), and $p < 0.0001$ (****).

that causes this increase in temperature.[40] This study shows that the use of a catalyst can significantly lower the CO concentration.

3.3. Particulate Matter Emission. The mass concentration of total suspended particles (TSP) was measured according to the EN16510 standard. The measurement was conducted for each nominal cycle, and the global average was calculated. Figure 4c displays the averages for the Reference and the Catalyst along with their respective standard deviation values. Based on these concentrations, a significant reduction of 67% (p = 0.016) in the TSP mass concentration is observed when the catalyst is used.

The online measurement of PNSD, corrected at 13 vol% O_2, was multiplied by the dilution rate and averaged for the 5 loads for the Reference and the Catalyst (Figure 4d). Both PNSDs are unimodal, showing a peak around 100 nm, as referenced in the literature,[5] with a base width from 0.04 to 0.8 μm. No significant difference (p = 0.57) can be observed between these two PNSDs. As the measurements were not isokinetically conducted, the sampling errors for particles larger than 1 μm might exceed 1%, making it challenging to provide a conclusive statement regarding the largest particles only from the ELPI+ measurement.[30]

3.4. Water-Soluble Condensable Organic Compounds (WSCOC). Collected condensates were characterized prior to their use in the cytotoxic study. Figure S5 shows the visual aspect of the condensates harvested with and without the catalyst. A clear difference is observable where the solution is brownish in the absence of a catalyst and clear when a catalyst is used. TOC of condensates was measured to evaluate the gas equivalent concentration of WSCOC and the impact of the catalyst on these compounds. The results are shown in Figure 4c. Based on these concentrations, the catalytic conversion rate of WSCOC was calculated at 80%.

The concentrations of 16 U.S. EPA priority PAH pollutants have been measured in the collected condensates, and their equivalent concentrations in the gas phase are reported in Table S2. PAH concentration was summed and shown in

https://doi.org/10.1021/acsomega.5c00854
ACS Omega 2025, 10, 25506−25517

Figure 4b; the catalytic conversion of PAH was calculated at around 94%. It is most noticeable that a high conversion performance was observed for most of the identified molecules.

Overall, the tested catalyst has shown high efficiency in reducing polluting emissions from wood stoves, notably, CO, TSP, WSCOC, and PAH. Despite its proven efficiencies, addressing the remaining cytotoxicity is necessary.

3.5. Cytotoxicity Study. In this study, we chose to evaluate the toxicity of WSCOC instead of PM, based on the findings of our preliminary investigation detailed in Section 2.5.1 of the Supporting Information. Notably, no significant short-term cytotoxicity has been associated with exposure to high concentrations of medium suspended PM. Therefore, to quantify the difference in cytotoxicity achieved using a catalyst, condensates have been converted to culture media and cells were exposed to WSCOC-containing culture media for 24 h. A dose−response was evaluated by diluting the main solution, and the selected relative WSCOC concentrations were 0.00 (or control), 0.05, 0.10, 0.25, 0.50, 0.75, and 1.00. As a first and simple method of evaluation, the cell morphology has been observed through an inverse optical microscope after 24 h of exposure, and these micrographs are shown in Figure 5. A clear difference in morphology is observed for the cells in Reference. Moreover, multiple blebs (see red arrows in Figure 5) are formed on the cells, which are signs of cell suffering.

Live and dead assays were conducted to evaluate cell mortality after exposure to the collected WSCOC. The results of these assays are listed in Figure 6a.

A dose−response is observed for both the Reference and the catalyst, but only the cells exposed to WSCOC from Reference sampling reach almost 100% mortality rate. This high mortality rate observed in the Reference compared to the Catalyst suggests that the WSCOC are significantly ($p < 0.001$) more cytotoxic in the absence of the catalyst.

The cell metabolic activity after exposure to the collected condensates was evaluated by MTT. Figure 6b shows the results of the metabolic activity of cells exposed to different relative WSCOC concentrations. A dose−response is observed for both the Reference and the Catalyst, but a sharper decrease in metabolic activity is observed for the cells exposed to the WSCOC from the Reference, where a statistically significant difference is observed from 0.10 to 1.00 of relative WSCOC concentration (p-values corrected are the following: 0.05 $p = 1$; 0.10 $p = 0.0031$; 0.25 $p < 0.0001$; 0.50 $p = 0.005$; 1.00 $p = 0.0045$). This lower metabolic activity for the Reference confirms the higher cytotoxicity of the WSCOC collected in the absence of the catalyst.

4. DISCUSSION

According to the EN16510 standard, the catalyst appears to have a significant effect on decreasing CO concentrations, a moderate impact on the mass concentration of TSP, and a less than moderate influence on the concentration of the OGC concentration. When compared to the recent results reported by Ryšavý et al.,[20] where their conversion efficiencies are 88% for CO, 37% for OGC, and 25% for TSP, our findings (89% for CO, 17% for OGC, and 67% for TSP) are largely consistent, with the exception of a notably enhanced TSP removal in our study. However, upon further investigation, it became evident that the catalyst's effectiveness extends beyond the parameters assessed by the European standard.

A difference in the catalytic conversion between different types of organic species is observed. WSCOC, a subgroup of OGC with lower saturating vapor pressure and better affinity with water, is easily converted to CO_2. Meaning that the remaining subgroup called: "High-Saturating Vapor Organic Compound" (HSVOC) is, on average, hardly converted into CO_2. Knowing the average concentration in the presence and absence of the catalyst, the HSVOC concentration can be estimated by subtracting WSCOC from the concentration of the OGC. The concentrations of HSVOC are, respectively, 120 and 121 mgC/Nm^3 for the Reference and Catalyst, indicating a minimal impact on this subgroup by the catalyst. Identifying specific molecules within this subgroup is challenging without analytical measurements, but clues are given from their physicochemical characteristics. Petterson et al. have conducted measurements on a wood stove, revealing methane, ethene, and acetylene as the OGC predominant components.[41] Additionally, Pieber et al. have confirmed a low catalytic conversion rate for methane below 600 °C,[17] suggesting a significant contribution of methane to the HSVOC subgroup, which is a nontoxic species. The low catalytic conversion rate of methane, combined with its high concentration within the OGC group, explains why the overall OGC catalytic conversion of the OGC (±20%) is lower than that of CO (±90%). Moreover, an in vitro cytotoxic study has shown that the removal of WSCOC by the catalyst is followed by a decrease in acute short-term cytotoxicity. However, in the presence of the catalyst, a slight decline in metabolic activity was observed at high concentrations. This implies that cells still experience a degree of stress, which could impact the cell viability on a longer exposure period. In conclusion, we can confirm that the catalyst plays a major role in eliminating molecules with a high toxic impact on human health from the generated fumes. This decrease is an important step in the cleansing of the exhaust fumes generated by wood stoves.

The particulate emissions were assessed using two different methods, as presented in the preceding section. The impact of the catalyst on the mass concentration has shown a decrease of 66%, whereas the PNSD showed no difference when the catalyst is used. This difference can be related to the nature of the measurement technique. The particle diameter measuring range of ELPI+ is between 6 nm and 10 μm, thus having an upper limit, whereas the mass concentrations obtained by filtering do not. Even if the mode of PNSD is around 100 nm, as the mass is proportional to the cube of the particle diameter, the removal of a larger diameter particle will have a greater impact on the mass concentration than particles with a smaller diameter. Thus, when the PNSD shows no difference below 10 μm compared to the filter that has a 66% conversion, it is more likely that the particles removed by the catalyst have a diameter higher than the upper limit of detection of the ELPI+ (10 μm). Indeed, as seen in Figure S4, the bottom part of the catalyst is covered with black soot after a catalyst test, suggesting that coarse particles (i.e., >10 μm) have impacted on it. When the streamlines of the exhaust interact with the catalyst, large particles (at least the ones above 10 μm) will impact on the catalyst due to their larger inertia. On the other hand, smaller particles with less inertia may follow the streamlines and will not be deposited on the catalyst. Consequently, we hypothesize that the reduction in particle mass primarily stems from larger particles (>10 μm) that deposit on the catalyst surface, which falls beyond the measurement range of ELPI+.

https://doi.org/10.1021/acsomega.5c00854
ACS Omega 2025, 10, 25506−25517

5. CONCLUSIONS AND OUTLOOK

In this study, an in-house catalyst has shown its high efficiency in decreasing the concentration of pollutants such as carbon monoxide (87%). On organic species, a slight decrease was observed for the level of OGC (19%), but its WSCOC subgroup, containing the most toxic components, displayed a higher catalytic conversion rate (80%), and its low remaining short-term cytotoxicity was confirmed by the in vitro study. On the other hand, the HSVOC subgroup, which was slightly affected by the catalyst, is mostly composed of methane. Regarding particulate emissions, particles above 10 μm impact the catalyst and are responsible for the decrease of 67% in mass concentration. These results support this catalyst as an efficient integrated solution in wood stoves and as a CO_2-neutral technology pivotal for the European Union 2050 climate-neutrality objectives. Nevertheless, future research should address other issues to achieve this objective: (1) influence of the catalyst on methane concentration in real time needs to be evaluated; (2) remaining toxicity of OGC (and not only WSCOC) needs to be investigated; (3) investigation of catalyst effectiveness on an identified chemical species; and (4) evaluation of long-term performance and durability of the catalyst

■ ASSOCIATED CONTENT

Supporting Information

The Supporting Information is available free of charge at https://pubs.acs.org/doi/10.1021/acsomega.5c00854.

Additional experimental details on the wood chemical composition (Table S1), extended results on the temporal profiles of the combustion cycles (Figures S1 and S2), temperature inversion (Figure S3), visual aspect of the catalyst monolith (Figure S4), and WSCOC solutions (Figure S5) after the campaign, PAH concentrations (Table S2), logistic regression on A549 mortality (Figure S6), and the MTT assay on the impact of particulate matter on A549 cells (Figure S7) (PDF)

■ AUTHOR INFORMATION

Corresponding Authors

Marvin Laboureur − *Laboratory of Inorganic Materials Chemistry (CMI) − Namur Institute of Structured Matter (NISM), University of Namur, Namur 5000, Belgium; Stuv S.A., Floreffe 5150, Belgium;* orcid.org/0000-0002-2053-3870; Email: marvin.laboureur@unamur.be

Bao-Lian Su − *Laboratory of Inorganic Materials Chemistry (CMI) − Namur Institute of Structured Matter (NISM), University of Namur, Namur 5000, Belgium; State Key Laboratory of Advanced Technology for Materials Synthesis and Processing, Wuhan University of Technology, Wuhan 430070, China;* orcid.org/0000-0001-8474-0652; Email: bao-lian.su@unamur.be

Authors

Maxence Hannard − *Laboratory of Inorganic Materials Chemistry (CMI) − Namur Institute of Structured Matter (NISM), University of Namur, Namur 5000, Belgium; Empa - Swiss Federal Laboratories for Materials Science and Technology, Dübendorf 8600, Switzerland*

Tarek Barakat − *Laboratory of Inorganic Materials Chemistry (CMI) − Namur Institute of Structured Matter (NISM), University of Namur, Namur 5000, Belgium; Stuv S.A., Floreffe 5150, Belgium*

Abhishek Goel − *Thermo and Fluid Dynamics (FLOW), Vrije Universiteit Brussel (VUB), Brussels 1050, Belgium; Brussels Institute for Thermal-fluid Systems and Clean Energy (BRITE), Vrije Universiteit Brussel (VUB) and Université Libre de Bruxelles (ULB), Brussels 1050, Belgium;* orcid.org/0000-0003-0469-1745

Jordi Cornette − *Thermo and Fluid Dynamics (FLOW), Vrije Universiteit Brussel (VUB), Brussels 1050, Belgium; Brussels Institute for Thermal-fluid Systems and Clean Energy (BRITE), Vrije Universiteit Brussel (VUB) and Université Libre de Bruxelles (ULB), Brussels 1050, Belgium; Faculty of Aerospace Engineering, Delft University of Technology, Delft 2629 HS, The Netherlands;* orcid.org/0000-0003-0337-553X

Svend Bram − *Thermo and Fluid Dynamics (FLOW), Vrije Universiteit Brussel (VUB), Brussels 1050, Belgium; Brussels Institute for Thermal-fluid Systems and Clean Energy (BRITE), Vrije Universiteit Brussel (VUB) and Université Libre de Bruxelles (ULB), Brussels 1050, Belgium*

Patricia Renard − *Laboratory of Biochemistry and Cell Biology (URBC)-Namur Research Institute for Life Sciences (NARILIS), University of Namur, Namur 5000, Belgium*

Thomas Duquesne − *Stuv S.A., Floreffe 5150, Belgium*

Complete contact information is available at: https://pubs.acs.org/10.1021/acsomega.5c00854

Author Contributions

◆M.L. and M.H. contributed equally to this work. M.L.: Conceptualization, methodology, software, validation, formal analysis, investigation, resources, data curation, writing—original draft, visualization; M.H.: conceptualization, methodology, validation, formal analysis, investigation, data curation, writing—original draft, visualization; T.B. and A.G.: investigation, resources, writing—review and editing; J.C.: conceptualization, writing—review and editing; S.B.: resources, writing—review and editing; P.R.: conceptualization, resources, writing—review and editing; T.D. and B.-L.S.: resources, supervision, project administration, funding acquisition

Notes

The authors declare no competing financial interest.

■ ACKNOWLEDGMENTS

The authors thank the public service of Wallonia—SPW recherche ["*Doctorat en entreprise*"—Convention No. 8180] and Stûv S.A. for financial support, as well as the University of Namur and Stûv S.A. for technical and scientific support. The authors also thank the members of the URBC Laboratory of the University of Namur for the valuable scientific discussions and Olivia Bleeckx for her assistance in selecting the appropriate statistical tests and calculate the associated *p*-values.

■ REFERENCES

(1) EU Commission and others. A strategic long-term vision for a prosperous, modern, competitive & climate-neutral economy EU vision for 2050 − " A Clean Planet for All, " *European Commission* 2018; Vol. 773, pp 1−25.

(2) Bhattu, D.; Zotter, P.; Zhou, J.; Stefenelli, G.; Klein, F.; Bertrand, A.; Temime-Roussel, B.; Marchand, N.; Slowik, J. G.; Baltensperger, U.; Prévôt, A. S. H.; Nussbaumer, T.; El Haddad, I.; Dommen, J. Effect of Stove Technology and Combustion Conditions on Gas and

Particulate Emissions from Residential Biomass Combustion. *Environ. Sci. Technol.* **2019**, *53*, 2209−2219.
(3) Price-Allison, A.; Mason, P. E.; Jones, J. M.; Barimah, E. K.; Jose, G.; Brown, A. E.; Ross, A. B.; Williams, A. The Impact of Fuelwood Moisture Content on the Emission of Gaseous and Particulate Pollutants from a Wood Stove. *Combust. Sci. Technol.* **2021**, 1−20.
(4) Nussbaumer, T.; Doberer, A.; Klippel, N.; Bühler, R.; Vock, W.*Influence of Ignition and Operation Type on Particle Emissions From Residential Wood Combustion*, 16th European Biomass Conference and Exhibition; 2008; pp 2−6.
(5) Naeher, L. P.; Brauer, M.; Lipsett, M.; Zelikoff, J. T.; Simpson, C. D.; Koenig, J. Q.; Smith, K. R. Woodsmoke health effects: A review. *Inhalation Toxicol.* **2007**, *19*, 67−106.
(6) Forest Research, Carbon emissions of different fuels - Forest Research. 2021 https://www.forestresearch.gov.uk/tools-and-resources/fthr/biomass-energy-resources/reference-biomass/facts-figures/carbon-emissions-of-different-fuels/%0Ahttps://www.forestresearch.gov.uk/tools-and-resources/biomass-energy-resources/reference-biomass/fac (accessed Nov 21, 2023).
(7) Cohen, A. J.; Brauer, M.; Burnett, R.; Anderson, H. R.; Frostad, J.; Estep, K.; Balakrishnan, K.; Brunekreef, B.; Dandona, L.; Dandona, R.; Feigin, V.; Freedman, G.; Hubbell, B.; Jobling, A.; Kan, H.; Knibbs, L.; Liu, Y.; Martin, R.; Morawska, L.; Pope, C. A.; Shin, H.; Straif, K.; Shaddick, G.; Thomas, M.; van Dingenen, R.; van Donkelaar, A.; Vos, T.; Murray, C. J. L.; Forouzanfar, M. H. Estimates and 25-year trends of the global burden of disease attributable to ambient air pollution: an analysis of data from the Global Burden of Diseases Study 2015. *Lancet* **2017**, *389*, 1907−1918.
(8) Anderson, J. O.; Thundiyil, J. G.; Stolbach, A. Clearing the Air: A Review of the Effects of Particulate Matter Air Pollution on Human Health. *J. Med. Toxicol.* **2012**, *8*, 166−175.
(9) Betteridge, D. J. What is oxidative stress? *Metab., Clin. Exp.* **2000**, *49*, 3−8.
(10) Patel, A. B.; Shaikh, S.; Jain, K. R.; Desai, C.; Madamwar, D. Polycyclic Aromatic Hydrocarbons: Sources, Toxicity, and Remediation Approaches. *Front. Microbiol.* **2020**, *11*, No. 562813, DOI: 10.3389/fmicb.2020.562813.
(11) Ramos De Rainho, C.; MacHado Corrêa, S.; Luiz Mazzei, J.; Alessandra Fortes Aiub, C.; Felzenszwalb, I. Genotoxicity of polycyclic aromatic hydrocarbons and nitro-derived in respirable airborne particulate matter collected from urban areas of Rio de Janeiro (Brazil). *BioMed Res. Int.* **2013**, *2013*, No. 765352.
(12) Baird, W. M.; Hooven, L. A.; Mahadevan, B. Carcinogenic polycyclic aromatic hydrocarbon-DNA adducts and mechanism of action. *Environ. Mol. Mutagen.* **2005**, *45*, 106−114.
(13) Tang, Y.; Zhang, J. L. Recent developments in DNA adduct analysis using liquid chromatography coupled with mass spectrometry. *J. Sep. Sci.* **2020**, *43*, 31−55.
(14) Cottom, J. W.; Mitchell, E.; Lea-Langton, A.; Jones, J. Up in smoke The contribution of domestic outdoor burning to UK particulate matter emissions Executive summary. 2021.
(15) European Commission. (Text with EEA relevance) 21.06.2017, 2016. 2018, pp 48−119.
(16) Brandelet, B.; Rose, C.; Landreau, J.; Druette, L.; Rogaume, Y. Toward a cleaner domestic wood heating by the optimization of firewood stoves? *J. Cleaner Prod.* **2021**, *325*, No. 129338.
(17) Pieber, S. M.; Kambolis, A.; Ferri, D.; Bhattu, D.; Bruns, E. A. E. A.; Elsener, M.; Kröcher, O.; Prévôt, A.S.H.A.S.H.; Baltensperger, U. Mitigation of Secondary Organic Aerosol Formation from Log Wood Burning Emissions by Catalytic Removal of Aromatic Hydrocarbons. *Environ. Sci. Technol.* **2018**, *52*, 13381−13390.
(18) Kaivosoja, T.; Virén, A.; Tissari, J.; Ruuskanen, J.; Tarhanen, J.; Sippula, O.; Jokiniemi, J. Effects of a catalytic converter on PCDD/F, chlorophenol and PAH emissions in residential wood combustion. *Chemosphere* **2012**, *88*, 278−285.
(19) Vicente, E. D.; Duarte, M. A.; Tarelho, L. A. C.; Alves, C. A. Efficiency of Emission Reduction Technologies for Residential Biomass Combustion Appliances: Electrostatic Precipitator and Catalyst. *Energies* **2022**, *15*, No. 4066.
(20) Ryšavý, J.; Vicente, E. A. D.; Jaroch, M.; Alves, C. A.; Sánchez De La Campa, A.; Horák, J. Reducing the impact of biomass combustion in residential units on local air quality by using innovative low-loading Pt-based heterogeneous catalyst. *Biomass Bioenergy* **2024**, *183*, No. 107147.
(21) Jaworek, A.; Sobczyk, A. T.; Marchewicz, A.; Krupa, A.; Czech, T. Particulate matter emission control from small residential boilers after biomass combustion. A review. *Renewable Sustainable Energy Rev.* **2021**, *137*, No. 110446.
(22) Brunner, T.; Wuercher, G.; Obernberger, I. 2-Year field operation monitoring of electrostatic precipitators for residential wood heating systems. *Biomass Bioenergy* **2018**, *111*, 278−287.
(23) Schneider, E.; Czech, H.; Hartikainen, A.; Hansen, H. J.; Gawlitta, N.; Ihalainen, M.; Yli-Pirilä, P.; Somero, M.; Kortelainen, M.; Louhisalmi, J.; Orasche, J.; Fang, Z.; Rudich, Y.; Sippula, O.; Rüger, C. P.; Zimmermann, R. Molecular composition of fresh and aged aerosols from residential wood combustion and gasoline car with modern emission mitigation technology. *Environ. Sci.: Processes Impacts* **2024**, *26*, 1295−1309.
(24) Hosseini, M.; Barakat, T.; Cousin, R.; Aboukaïs, A.; Su, B.-L. L.; De Weireld, G.; Siffert, S. Catalytic performance of core-shell and alloy Pd-Au nanoparticles for total oxidation of VOC: The effect of metal deposition. *Appl. Catal., B* **2012**, *111*−*112*, 218−224.
(25) Idakiev, V.; Dimitrov, D.; Tabakova, T.; Ivanov, K.; Yuan, Z. Y.; Su, B. L. Catalytic abatement of CO and volatile organic compounds in waste gases by gold catalysts supported on ceria-modified mesoporous titania and zirconia, Cuihua Xuebao/. *Chin. J. Catal.* **2015**, *36*, 579−587.
(26) Zhang, J.; Xu, X.; Zhao, S.; Meng, X.; Xiao, F.-S. Recent advances of zeolites in catalytic oxidations of volatile organic compounds. *Catal. Today* **2023**, *410*, 56−67.
(27) Yu, B.; Deng, H.; Lu, Y.; Pan, T.; Shan, W.; He, H. Adsorptive interaction between typical VOCs and various topological zeolites: Mixture effect and mechanism. *J. Environ. Sci.* **2024**, *136*, 626−636.
(28) Barakat, T.; Su, B.-L. Process of Manufacture of a Solid Catalyst Made of a Support Coated with a Thin Catalytic Layer. CA3105254A1, 2020.
(29) Bindig, R.; Butt, S.; Hartmann, I.; Matthes, M.; Thiel, C. Application of heterogeneous catalysis in small-scale biomass combustion systems. *Catalysts* **2012**, *2*, 223−243.
(30) Cornette, J. F. P.; Dyakov, I. V.; Blondeau, J.; Bram, S. Accurate particulate matter emission measurements from biomass combustion : A holistic evaluation of full and partial flow dilution systems. *Environ. Res.* **2023**, *236*, No. 116714.
(31) Coudray, N.; Dieterlen, A.; Roth, E.; Trouvé, G. Density measurement of fine aerosol fractions from wood combustion sources using ELPI distributions and image processing techniques. *Fuel* **2009**, *88*, 947−954.
(32) Cornette, J. F. P.; Blondeau, J.; Bram, S. Influence of the dynamic behaviour of impactor surfaces on particulate matter emission measurements with electrical low pressure impactors. *Powder Technol.* **2023**, *419*, No. 118333.
(33) Zotter, P.; Richard, S.; Egli, M.; Rothen-Rutishauser, B.; Nussbaumer, T. A Simple Method to Determine Cytotoxicity of Water-Soluble Organic Compounds and Solid Particles from Biomass Combustion in Lung Cells in Vitro. *Environ. Sci. Technol.* **2019**, *53*, 3959−3968.
(34) Dilger, M.; Orasche, J.; Zimmermann, R.; Paur, H. R.; Diabaté, S.; Weiss, C. Toxicity of wood smoke particles in human A549 lung epithelial cells : the role of PAHs, soot and zinc. *Arch. Toxicol.* **2016**, *90*, 3029−3044.
(35) Danielsen, P. H.; Møller, P.; Jensen, K. A.; Sharma, A. K.; Wallin, H.; Bossi, R.; Autrup, H.; Mølhave, L.; Ravanat, J. L.; Briedé, J. J.; De Kok, T. M.; Loft, S. Oxidative stress, DNA damage, and inflammation induced by ambient air and wood smoke particulate matter in human A549 and THP-1 cell lines. *Chem. Res. Toxicol.* **2011**, *24*, 168−184.

(36) Figueiredo, D.; Vicente, E. D.; Gonçalves, C.; Lopes, I.; Oliveira, H.; Alves, C. A. Outdoor charcoal combustion in barbecue grills: Potential cytotoxic, oxidative stress and mutagenic effects. *Atmos. Environ.* **2024**, *322*, No. 120383.
(37) Shah, P. M.; Burnett, J. W. H.; Morgan, D. J.; Davies, T. E.; Taylor, S. H. Ceria−Zirconia Mixed Metal Oxides Prepared via Mechanochemical Grinding of Carbonates for the Total Oxidation of Propane and Naphthalene. *Catalysts* **2019**, *9*, No. 475.
(38) Reddy, B. M.; Khan, A. Nanosized CeO2−SiO2, CeO2−TiO2, and CeO2−ZrO2Mixed Oxides: Influence of Supporting Oxide on Thermal Stability and Oxygen Storage Properties of Ceria. *Catal. Surv Asia* **2005**, *9*, 155−171.
(39) Marinho, A. L. A.; Rabelo-Neto, R. C.; Epron, F.; Bion, N.; Noronha, F. B.; Toniolo, F. S. Pt nanoparticles embedded in CeO2 and CeZrO2 catalysts for biogas upgrading: Investigation on carbon removal mechanism by oxygen isotopic exchange and DRIFTS. *J. CO2 Util.* **2021**, *49*, No. 101572.
(40) Raj, R.; Harold, M. P.; Balakotaiah, V. Steady-state and dynamic hysteresis effects during lean co-oxidation of CO and C3H6 over Pt/Al2O3 monolithic catalyst. *Chem. Eng. J.* **2015**, *281*, 322−333.
(41) Pettersson, E.; Boman, C.; Westerholm, R.; Boström, D.; Nordin, A.; Pettersson, E.; Westerholm, R.; Boström, D.; Nordin, A. Stove performance and emission characteristics in residential wood log and pellet combustion, part 1: Pellet stoves. *Energy Fuels* **2011**, *25*, 307−314.

https://doi.org/10.1021/acsomega.5c00854
ACS Omega 2025, 10, 25506−25517